HHS Public Access

Author manuscript

Appl Opt. Author manuscript; available in PMC 2019 June 26.

Published in final edited form as:

Appl Opt. 2019 April 01; 58(10): C7–C13. doi:10.1364/AO.58.0000C7.

Velocimetry based on dye visualization for a pulsatile tubing flow measurement

ZIFENG YANG[*] and **MARK JOHNSON**

Department of Mechanical and Materials Engineering, Wright State University, 3640 Colonel Glenn Hwy., Dayton, Ohio 45435, USA

Abstract

A dye visualization experiment was designed and operated as an analogy of x-ray angiographic imaging. The velocimetry technique based on dye visualization for a pulsatile tubing flow measurement is introduced. The optical flow method was utilized to recover the velocity field from the visualization images. For the same flow condition, a digital particle image velocimetry (PIV) system was also employed to measure the same flow field in the middle plane. The purpose of this study was to determine the accuracy of the velocity field estimation from the transmittance-based two-dimensional projection image of the three-dimensional volumetric flow field by dye visualization in comparison with the PIV measurement results. Compared to the PIV results in the middle plane, the averaged velocity magnitude from the dye visualization measurement was underestimated by about 16%–24% in the central region and by about 29%–43% in the outer region across the tube at two time instants of the cyclic pulsatile flow.

1. INTRODUCTION

Blood flow velocimetry has drawn a great deal of interest from the medical engineering field. Blood flow velocity and associated hemodynamic factors, e.g., wall shear stress, have been identified as key factors causing several vascular diseases such as stenosis and aneurysms [1]. One of the promising techniques to obtain a blood flow map is x-ray video densitometric blood velocimetry based on x-ray angiographic imaging. During x-ray angiographic imaging, the contrast agent (usually iodine-based) is injected into the blood flow. As the contrast agent has a higher x-ray absorption coefficient than the surrounding blood cells and tissues, a darkness pattern associated with the contrast agent distribution will be visualized on the imaging plane through a scintillator [1,2]. Through detecting the radioopaque contrast agent in the blood flow, the movement of the blood flow can be estimated by using the optical flow method (OFM) [3,4].

The optical flow algorithm to recover the apparent motion of the image brightness patterns has drawn a great deal of interest from many research groups from the fields of computer vision, fluid mechanics, meteorology, and medical imaging [5–9]. The OFM for estimating 2D flow from both particle images and patterned (texture) images has been well validated by various groups [3,7]. Some research groups from the medical field have utilized OFM for

[*]*Corresponding author:* zifeng.yang@wright.edu.

velocity estimation from x-ray angiographic images and magnetic resonance angiographic images of human blood vessels [10–12]. These measurement results were essentially used to validate or compare with computational fluid dynamic results. However, very little research on the validation of the video densitometric velocimetry technique for internal velocity field measurements can be found in the literature. Pereira *et al.* [13] tested the reliability of the OFM for digital subtraction angiography, and the measurement results were essentially validated in terms of volume flow rate with Doppler sonography. There is still a lack of validation in terms of detailed flow field comparison. Wildes *et al.* [14] set up a microscale x-ray imaging rig to acquire an image sequence of steady flow in a micro-scale fluidic device with the emulsified contrast medium (not soluble) pre-dispersed in the fluid. The velocity estimation from cinematic sequential images agreed with theoretical prediction for fully developed flow in a micropipe flow. Neither the dimension nor the contrast medium diffusion manner in this study represented the realistic x-ray angiographic blood velocimetry.

The optical flow algorithm is capable of recovering twoP-dimensional optical flow from successive angiographic images of the physical flow, but how well this recovered velocity field represents the three-dimensional volumetric field is still an open question. The present research focused on the comparative flow measurements using both the dye visualization technique based on transmittance light and the PIV technique for a pulsatile tubing flow, which has the essential feature of blood flow. Visualization 1 of the soluble dye injected into the water flow, taking advantage of the transmittance of visible light, served as the analogy of the x-ray angiographic imaging process. The results from the dye visualization measurements were compared with the PIV flow measurements in the middle plane of the tube at different time instants for a pulsatile flow. The purpose of this study was to quantify the accuracy of velocity field estimation from the transmittance-based two-dimensional projection image of the three-dimensional volumetric flow field in comparison with the PIV measurements.

2. EXPERIMENTAL SETUP

A. Dye Visualization Experiment

As shown in Fig. 1, a physiological blood flow phantom has been built with a pulsatile pump (Harvard Apparatus pulsatile blood pump for large animals), two reservoirs, bifurcate connectors, and Tygon tubing. The pulsatile pump creates waveforms similar to cardiac flows. The nominal average flow rate of 20 mL/s, a pulse rate of 55 Hz, and ratio of systole to diastole of 35/65 is adjusted to match human condition. A syringe pump (Harvard Apparatus 11 Plus) with a constant flow rate of 20 mL/min is used to inject the red dye into the flow. The fluorescent red dye (rhodamine WT, Cole-Parmer) is noncarcinogenic. A 0.8 mm (1/32 inch) diameter (inner) tube serving as the catheter is inserted just upstream of the test section to allow injection of the red dye with an approximate concentration of 5000 ppm (parts per million). A spiral fixture ring is used to fix the position of the catheter in the cross section of the Tygon tube. The tube in the test section has an outer diameter of 12.7 mm (½ inch) and inner diameter of 9.5 mm (3/8 inch). A clear mainstream flow is required to make the dye flow more distinct; thus, the flow cannot be circulated. Instead, an open-circuit

tubing flow is set up for the dye visualization experiment; thus, two reservoirs are used in this experiment. The measurement is conducted under stable cyclic pulsatile flow conditions (constant pulse rate and steady volume flow waveform). Water bath is maintained at room temperature of 20 ± 0.5°C.

A visualization system including a bulb light source with a light diffuser sheet and a complementary metal-oxide semiconductor (CMOS) high-speed camera (TSI, Powerview HS-2000) is used to capture the transmittance-based visualization images continuously at a frame rate of 2000 frame/sec. By introducing the diffuser sheet in front of the light bulb, the intensity of light becomes more uniform and therefore mitigates intensity-caused error when using the optical flow algorithm to analyze images. The camera was triggered by a pulsed signal from a laser tachometer (Monarch, PLT200) detecting the cyclic motion of the pump. Therefore, the starting time instant relative to the cyclic pulsatile flow was fixed for all experimental trials. The camera image plane size was set as 1024 × 256 pixel (87 × 22 mm) to fit the current tubing flow, which allowed for over 4000 images to be collected at a time. By repeating the same process, 200 trials of the dye visualization experiments were carried out in order to obtain the averaged velocity field for each time step. Time-resolved velocity fields were estimated from the cinema sequence of 4000 images within 2 s for each trial by using the optical flow method. The mean velocity field was calculated by averaging the instantaneous velocity at each time step for 200 trials.

B. Optical Flow Method for Velocity Estimation

The optical flow method calculates the apparent movement of the intensity pattern in an image based on the conservation of image brightness at a point [5], so that

$$\frac{\partial I}{\partial t} + \vec{V} \cdot \nabla I = 0, \quad (1)$$

where I represents the image brightness in each pixel, $\vec{V}$ represents the optical flow velocity vector, and t represents time. By considering the physical effect [7], the governing equation was improved as

$$\frac{\partial I}{\partial t} + \vec{V} \cdot \nabla I + I \nabla \cdot \vec{V} = D \nabla^2 I, \quad (2)$$

where $\boldsymbol{I} \nabla \cdot \vec{\boldsymbol{V}}$ represents the divergence effect of the optical flow, $\boldsymbol{D} \nabla^2 \boldsymbol{I}$ represents the diffusion effect of the quantity in the flow such as the contrast density, and $\boldsymbol{D}$ is the diffusion coefficient. In the current experiment, $\boldsymbol{D}$ is assumed as zero because the diffusion velocity is much smaller than the mainstream flow velocity. Accordingly, using the calculus of variation to minimize the total error in Eq. (2), the Euler–Lagrange equation can be derived as

$$I \nabla \left[\partial I / \partial t + \vec{V} \cdot \nabla I + I \nabla \cdot \vec{V} - D \nabla^2 I \right] + \alpha \nabla^2 \vec{V} = 0, \quad (3)$$

where α is a constant weighting factor. A second-order five-point discrete scheme was developed to solve the velocity vectors from Eq. (3) numerically. The linear system can be solved by using Jacobi's blockwise iteration method. The converging iteration process ends when the remaining error is smaller than a preset small value. More details about this optical flow method can be referred to in our previously published work [3]. This divergence compensatory OFM has demonstrated more accurate velocity results using the same pattern images compared to the standard OFM [3,7]. The uncertainty of the velocity vector estimation, on average, was estimated as 1% of the optical flow velocity within the visualization image.

C. PIV Experiment

All settings for the pulsatile flow condition for the PIV experiment were maintained the same as for dye visualization. Instead of dye being injected through the catheter, the syringe was filled with a mixture of water and fluorescent particles. Since the PIV method required the illumination of particles, the flow downstream of the injection region was discharged back into the supply tank to conserve particles.

As shown in Fig. 2, a digital PIV system was employed to make the flow measurement in the middle plane of the tubing flow. The flow was seeded by fluorescent particles (fluorescent red polyethylene microspheres) with an averaged diameter of 10 ~ 45 μm and a density of 0.996 kg⁄m^3. A double-pulsed Nd: Yag laser (New Wave Gemini 120) was employed to provide two laser pulses of 120 mJ at a wavelength of 532 nm. Laser sheets were produced by a set of spherical and cylindrical lenses. A mirror was used to redirect the laser sheet to illuminate the flow in the tube. The laser sheet thickness in the measurement region was about 0.5 mm. The fluorescent particles were excited by the laser and emitted fluorescent light at a centered wavelength of 610 nm. A 14-bit charge-coupled device (CCD) camera (PCO, Pixelfly QE) with a resolution of 1392 × 1040 pixels (66 × 49 mm) was used for the double-image acquisition with the axis of the camera perpendicular to the measurement plane. A long-pass optic filter (transmission >600 nm) was installed on the lens of the camera to filter out the laser illumination and reflection. This method can significantly reduce the effect of light reflection from tube boundaries on the particle image. Since the maximum repetition rate of the laser was about 15 Hz, time-resolved measurements on the pulsatile flow could not be obtained. Therefore, a phase-locked PIV technique was utilized to get phase-averaged flow measurements for the pulsatile flow. To accomplish this, a tachometer was used to detect the cyclic motion of the pump, and two digital delay generators were used to synchronize the whole PIV system with the cyclic flow. The pulse signal from the laser tachometer triggered the first digital delay generator (Stanford Research Systems, Model DG535), which added a given time delay controlling the time phase, and then the first generator produced a pulse signal to trigger the second digital delay generator (Berkeley Nucleonics Corp, Model 575). The second digital delay generator controlled the whole PIV system and synchronized the double-pulsed laser and the CCD camera imaging process. Through this technique, the particle image was taken at the same timing (phase) relative to the cyclic pulsatile flow for all successive images. The camera was connected to a workstation for image view and storage.

Insight 4G software (TSI Inc.) was used to obtain instantaneous velocity vectors through a frame-to-frame cross-correlation methodology for particle image patterns in an interrogation window size of 32 × 32 pixel. An effective overlap of 50% was used for cross-correlation processing. After the instantaneous velocity was determined, phase-averaged velocity was obtained by averaging the cinema sequence of 200 frames of the instantaneous velocity field at the same phase as the pulsatile flow. The uncertainty for velocity vector measurements was estimated as 2% of velocity magnitude.

3. RESULTS

A. Images

Figure 3 shows the dye visualization image for optical flow analysis and the particle images for PIV analysis. For the dye visualization image [Fig. 3(a)], the distribution of the dye was observed in the middle region of the tube. Due to the turbulent effect and diffusion, the dye was successfully diffused and filled into the whole cross section. It should be noted that the flow in the tube was not a typical fully developed pipe flow; instead, the flow was unsteady and turbulent. Although the dye infusion through the catheter was continuous with a constant flow rate, as the pressure inside the tube and the velocity of the flow suddenly increased due to the pulsatile feature, the dye did not flow out of the catheter for a short time interval. Therefore, a blank region without dye was observed right downstream of the catheter for the current time instant $t/T = 0.2$, where t represents a time instant, and T represents the time period of the cyclic pulsatile flow. The similar pattern of dye distribution was also observed in the particle image from the PIV measurements as shown in Fig. 3(b). It can be observed that the right end of the tube was slightly tilted up for better diffusion of the dye. This was not observed in the dye visualization image in Fig. 3(a) because the camera was adjusted at an angle to show a horizontal tube in the image. The final PIV results were re-oriented as a horizontal tube to compare with the dye visualization results.

B. Volume Flow Rate Waveform

For phase-locked PIV measurements, 10 time instants from $t/T = 0 \sim 0.9$, with a step size of 0.1, were selected for velocity measurements. Averaged volume flow rate calculated based on the averaged velocity is plotted in Fig. 4. For the dye visualization measurements, as the camera view size was limited, at some time instant such as $t/T = 0.3$, the dye completely moved out of the camera window due to the sudden change in velocity and pressure, so this case cannot be used to estimate velocity. For some other time instants when the moving velocity was too low, the dye could not diffuse effectively into the whole cross section. Therefore, only two time instants, as two blue dots indicate in Fig. 4, were selected for velocity distribution comparison.

C. Flow Field and Velocity Profiles Comparison

Figure 5(a) shows the instantaneous velocity field estimated by the OFM on the dye visualization image at $t/T = 0.2$. The velocity vectors were superimposed on top of the dye image, so the correlation between dye distribution and velocity distribution can be clearly seen. The velocity vectors estimated by OFM had a high resolution, i.e., one vector per pixel. To visualize the vectors in a better fashion, 8 × 8 pixels were skipped to show the

vectors in Figs. 5(a)–5(c). In the region of uniform dye distribution, e.g., in the region from $X = 0$ to $X = 14$ mm, the velocity vectors cannot be calculated correctly, i.e., the movement of the brightness pattern cannot be discerned. In the region between $X = 16$ mm and $X = 42$ mm, the brightness pattern is good for velocity estimation, but in the region after $X = 44$ mm, very little dye can be observed; thus; poor velocity distribution was calculated. The velocity recovered from the OFM highly depends on the quality of the brightness distribution in the dye visualization image. Figure 5(b) shows the velocity distribution with velocity magnitude contours. In general, the high-speed region is well correlated with the good-quality brightness distribution, and this region is the so-called "effective region." Figure 5(c) presents the averaged velocity distribution at the same time instant from 200 trials of dye visualization measurements. Compared to the phase-averaged PIV measurement results shown in Fig. 5(d), the velocity magnitude in the effective region from the dye visualization measurements is lower. A quantitative comparison of the velocity profiles at two locations indicated by the blue dashed lines is presented in Figs. 6(a) and 6(b). The averaged velocity profile together with two instantaneous velocity profiles from the OFM are compared with the averaged velocity profile from the PIV measurements at $X = 34$ mm and $X = 42$ mm. At both locations, in the central region between $Y = -3$ mm and $Y = +3$ mm, the OFM results underestimate velocity magnitude by 0.1 m/s approximately, which corresponds to about 20% of the velocity magnitude of the PIV measurements. Outside the central region, as indicated by the black box region shown in Fig. 6, the OFM results underestimate velocity magnitude by 25% to 60% of the PIV measurements.

The reason for this large discrepancy is attributed mainly to the thick wall effect. This thick wall effect is depicted and explained by the diagram in Fig. 7. As shown in the shaded region, the light has to pass through two relatively thick walls, two low-speed regions, and a relatively high-speed region to generate projection of the dye image. As the two low-speed regions are adjacent to the high-speed region, the brightness pattern of the high-speed region is significantly affected by the dye distribution in the two neighboring low-speed regions. Therefore, a consistent underestimation of the flow velocity is obtained in all cases. It should be noted that the current experiment serves as an analogy of x-ray angiography. For x-ray angiography, the thick wall effect from the blood vessel would be less significant, since the penetrability of x-ray is substantially higher than visible light.

Instantaneous velocity profiles for the two time instants were also compared with the PIV results in Fig. 6. At both locations, the instantaneous velocity can match the PIV velocity profile at some region for some instances, while it can also produce a much lower velocity profile for some other instances. The comparison implies a significantly unstable distribution of the dye within the tube. If the distribution of the dye is in a thin layer close to the middle plane, which is also the PIV measurement plane, the velocity estimated from the dye visualization tends to agree with the PIV results well. When the dye distribution is off the middle plane, the velocity estimation is lower than the PIV results. By averaging all instances, velocity estimation based on dye visualization is always lower than the PIV measurement results in the middle plane.

Figure 8 shows the velocity measurement results from both dye visualization and PIV at $t/T = 0.5$, which represents the end of systole flow, and the beginning of diastole flow. To

visualize the vectors in a better fashion, 8 × 8 pixels were skipped to show the vectors in Figs. 8(a)–8(c). At this transition time instant, as shown in PIV results in Fig. 8(d), half of the tube flow above the centerline maintained a relatively high velocity, while the half below the centerline slowed down due to the reduced propulsion pressure. This phenomenon is also presented in the dye visualization image in Fig. 8(a), as a sparse amount of dye is diffused into the region below the centerline. As the pressure inside the flow decreases according to the waveform, the dye flowing out of the catheter diffuses well downstream of the catheter. As shown in Fig. 8(b), the high-speed region extends until the end of the current window. A very low-speed region below the centerline is caused mainly by the extremely low concentration of dye. This feature is also shown in the averaged results in Fig. 8(c).

The quantitative comparison of the velocity profiles at $X = 34$ mm is presented in Fig. 9. The dye visualization results do not capture the high-speed region above the centerline well. The averaged result from the dye visualization underestimates the velocity by 15%–45% between $y = 0$ mm and $y = 2.5$ mm, and by 3%–15% between $y = -3$ mm and $y = 0$ mm. In the region near the wall as indicated by the black box, the OFM results underestimate the velocity magnitude by 35% to 80% of the PIV measurements for this case.

The averaged velocity magnitude was calculated for both the central region ($|y| \leq 3$ mm) and the outer region ($|y| \leq 3$ mm), and the total volume flow rate was also calculated, based on the velocity profile at X 34 mm for $t/T = 0.2$ and 0.5 from both the dye visualization and PIV measurements. The results are summarized in Table 1. The estimated error in the averaged velocity magnitude for the central region is about 16% for the case of $t/T = 0.2$, and about 24% for the case of $t/T = 0.5$. In the outer region, the estimated error in the averaged velocity magnitude is about 29% for the case of $t/T = 0.2$ and 43% for the case of $t/T = 0.5$. The error in the total volume flow is approximately 18% and 32%, respectively.

Based on the comparison results between the dye visualization method and PIV measurements, although there is some discrepancy, we can still see the potential of the visualization technique based on transmittance imaging for flow velocity quantification, which is particularly meaningful for many medical imaging applications. Inherently, transmittance-based imaging has its shortcoming by projecting the three-dimensional volumetric distribution of the dye into a two-dimensional plane for OFM analysis. This compression effect from three-dimensional to two-dimensional field results in a lower velocity estimation compared with the middle plane velocity distribution, which has been observed from the present experiment. The improvement in velocity results based on transmittance imaging can fall into two folds: 1. Improving the diffusion and distribution of the dye can produce a better-quality image with a more discernable brightness pattern, which can increase the accuracy of OFM analysis. 2. Deriving correction modeling can correct velocity magnitude [15], which requires contribution from both numerical simulations and experimental results.

4. CONCLUSION

Although velocity field recovered from medical x-ray angiographic images and magnetic resonance images with OFM have been widely used for blood flow analysis and validation

of computational fluid dynamics simulations on hemodynamics, there is still a lack of solid validation of this technique for blood flow quantification. The inherent drawback of the transmittance-based image is that the three-dimensional volumetric flow field is projected onto a two-dimensional image plane. A dye visualization experiment in tubing flow was conducted as an analogy of the x-ray angiographic imaging process. The accuracy of the velocity field for a pulsatile tubing flow recovered from the dye visualization images based on transmittance light was estimated by comparing the results with the PIV measurements in the middle plane. It has been observed that mean velocity in the central region was underestimated by approximately 16%– 24% on average. But outside the central region, mean velocity was underestimated by about 29%–43%, which is attributed mainly to the thick wall effect. This effect is less significant for x-ray angiography due to the excellent penetrability of x-ray. Improvement of the accuracy of velocity recovery might be achieved by improving the diffusion and distribution of the dye in the flow and applying an appropriate correction model to correct velocity magnitude.

Acknowledgment.

The authors would like to acknowledge Mr. Pranay Sunil Pawar for his help in the early stage of the setup of this experiment.

Funding. National Heart, Lung, and Blood Institute (NHLBI) (R44HL132664).

REFERENCES

1. Shpilfoygel SD, Close RA, Valentino DJ, and Duckwiler GR, “X-ray video densitometric methods for blood flow and velocity measurement: a critical review of literature,” Med. Phys 27, 2008–2023 (2000). [PubMed: 11011728]
2. Fouras A, Kitchen MJ, Dubsky S, Lewis RA, Hooper SB, and Hourigan K, “The past, present and future of x-ray technology for in vivo imaging of function and form,” J. Appl. Phys 105, 102009 (2009).
3. Yang Z, Yu H, Huang G, and Ludwig B, “Divergence compensatory optical flow method for blood velocimetry,” J. Biomed. Eng 139, 061005 (2017).
4. Yang Z, “Optical flow method for blood flow velocimetry based on digital x-ray subtraction angiography: a brief review,” Res. Rev.: J. Med. Health Sci 6, 8–12 (2017).
5. Horn BK and Schunck BG, “Determining optical flow,” Artif. Intell 17, 185–203 (1981).
6. Corpetti T, Heitz D, Arroyo G, Memin E, and Santa-Cruz A, “Fluid experimental flow estimation based on an optical flow scheme,” Exp. Fluids 40, 80–97 (2006).
7. Liu T and Shen L, “Fluid flow and optical flow,” J. Fluid Mech 614, 253–291 (2008).
8. Liu T, Merat A, Makhmalbaf H, and Merati P, “Comparison between optical flow and cross-correlation methods for extraction of velocity field from particle images,” Exp. Fluids 56, 166 (2015).
9. Rhode K, Lambrou T, Hawkes D, and Seifalian A, “Novel approaches to the measurement of arterial blood flow from dynamic digital x-ray images,” IEEE Trans. Med. Imaging 24, 500–513 (2005). [PubMed: 15822808]
10. Bonnefous O, Pereira V, Ouared R, Rrina O, Aerts H, Hermans R, Nijnatten F, Stawiaski J, and Ruijters D, “Quantification of arterial flow using digital subtraction angiography,” Med. Phys 39, 6264–6275 (2012). [PubMed: 23039662]
11. Huang T, Wu T, Lin Y, Guo W, Huang W, and Lin C, “Quantitative flow measurements by digital subtraction angiography in cerebral carotid stenosis using optical flow method,” J. X-Ray Sci. Technol 21, 227–235 (2013).

12. Brina O, Ouared R, Bonnefous O, van Nijnatten F, Bouillot P, Bijlenga P, Schaller K, Lovblad K, Grunhagen T, Ruijters D, and Pereira V, “Intra-aneurysmal flow patterns: illustrative comparison among digital subtraction angiography, optical flow, and computational fluid dynamics,” AJNR Am. J. Neuroradiol 35, 2348–2353 (2014). [PubMed: 25082824]
13. Pereira VM, Ouared R, Brian O, Bonnefous O, Satwiaski J, Aerts H, Ruijters D, van Nijnatten F, Perren F, Bijlenga P, Schaller K, and Lovblad KO, “Quantification of internal carotid artery flow with digital subtraction angiography: validation of an optical flow approach with Doppler ultrasound,” AJNR Am. J. Neuroradiol 35, 156–163 (2014). [PubMed: 23928145]
14. Wildes RP, Amabile MJ, Lanzillotto AM, and Leu TS, “Recovering estimates of fluid flow from image sequence data,” Comput. Vis. Image Underst 80, 246–266 (2000).
15. Park H, Jung SY, Park JH, Kim JH, and Lee SJ, “Enhancement of measurement accuracy of x-ray PIV in comparison with the micro-PIV technique,” J. Synchrotron Radiat 25, 552–559 (2018). [PubMed: 29488936]

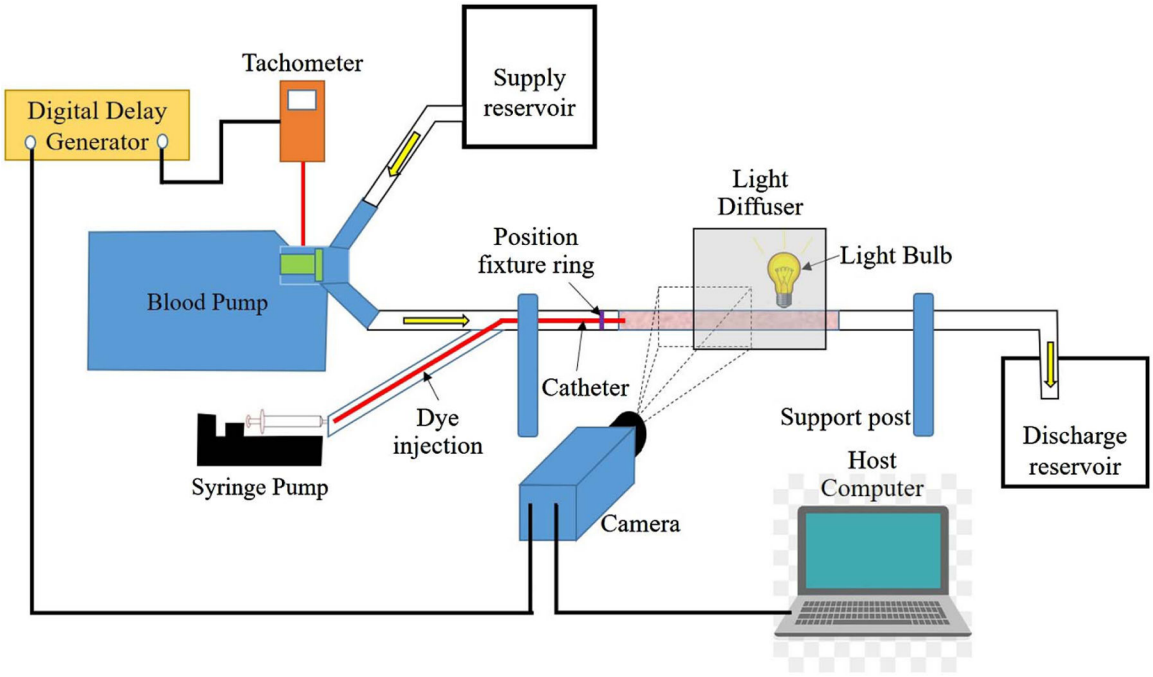

Fig. 1.
Dye visualization experimental setup.

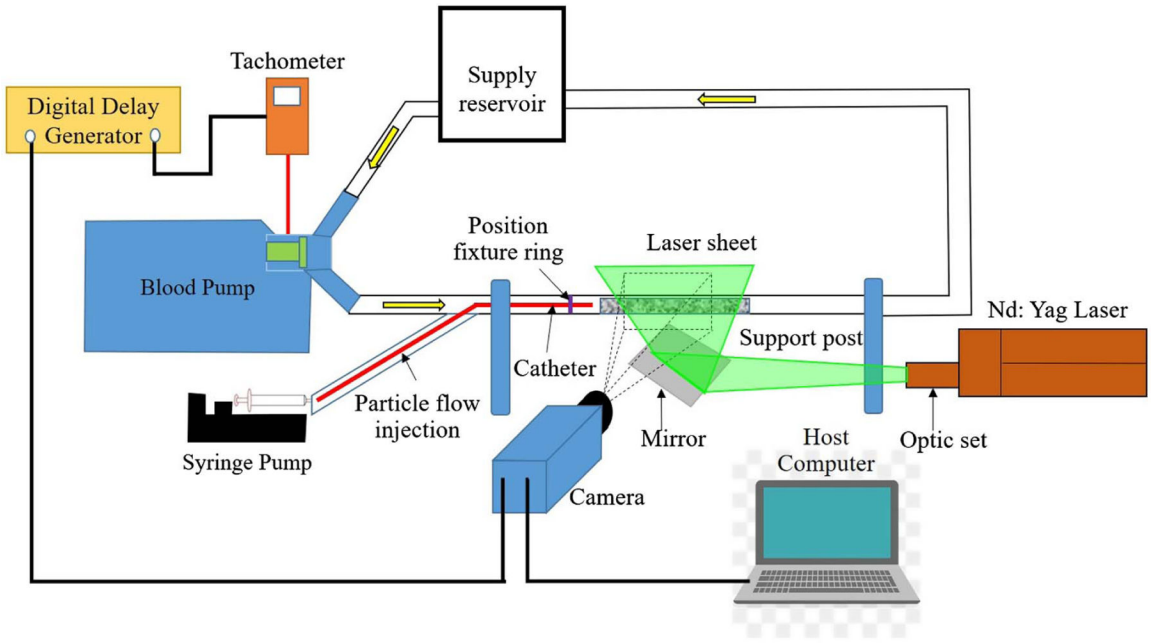

Fig. 2.
Experimental setup for PIV measurements.

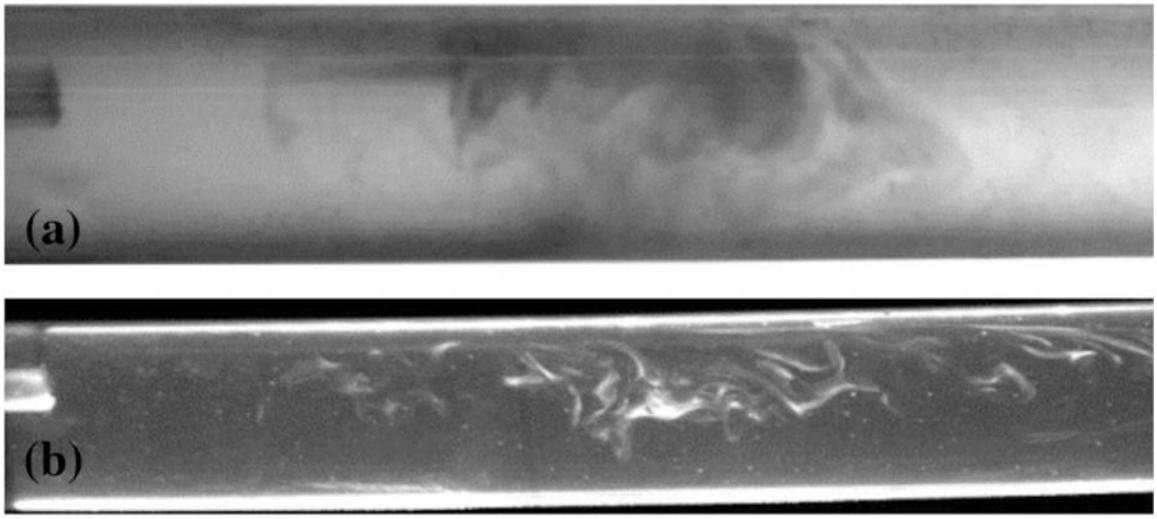

Fig. 3.

(a) Dye visualization image at $t/T = 0.2$; (b) particle image from PIV measurements at $t/T = 0.2$.

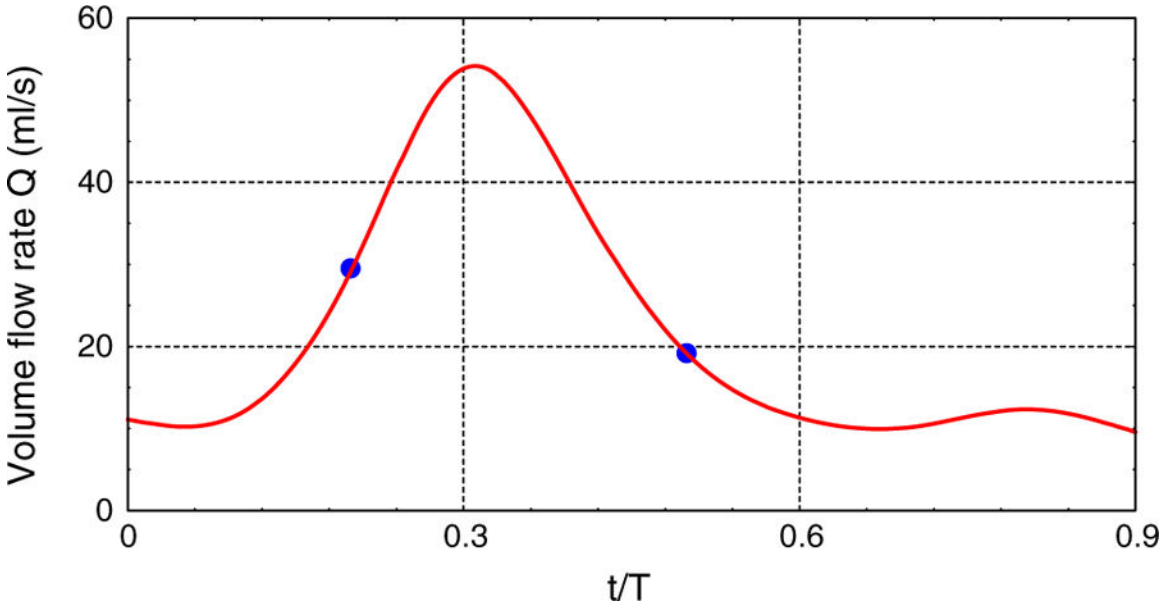

Fig. 4.
Volume flow rate waveform of the pulsatile flow.

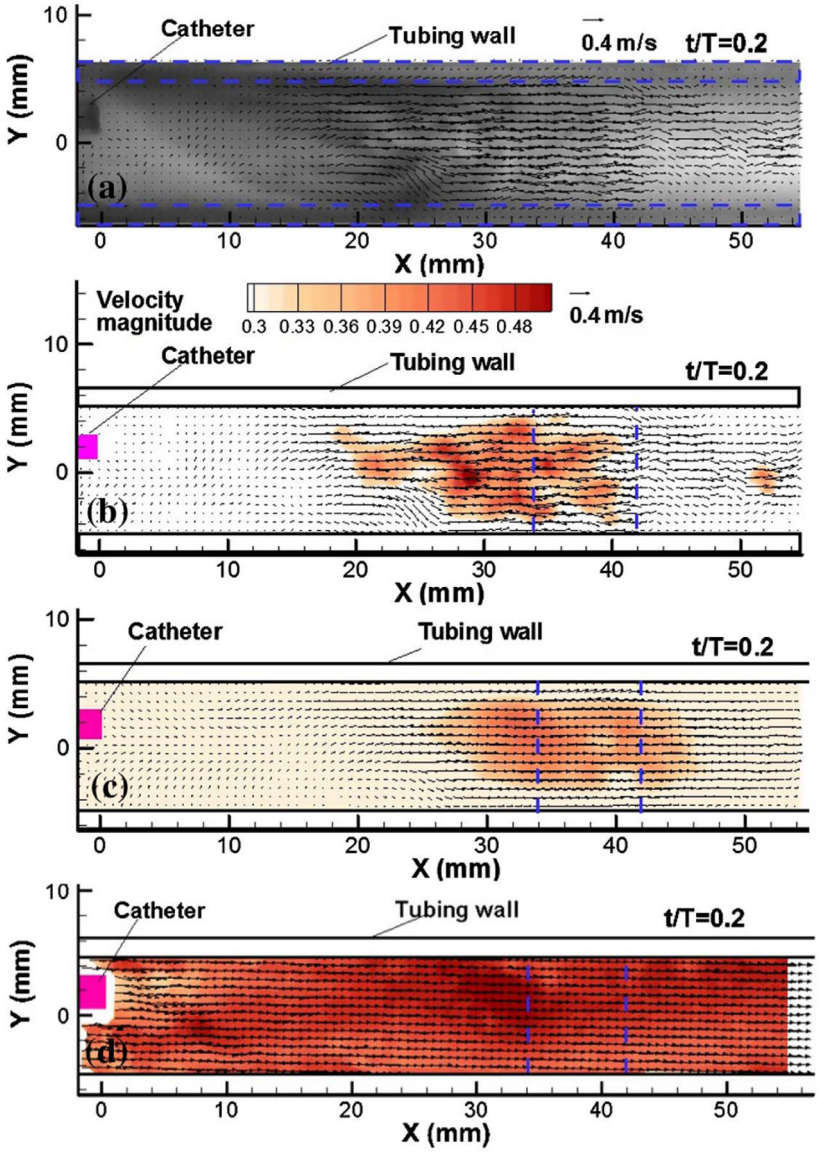

Fig. 5.

Velocity distribution results from OFM and PIV at $t/T = 0.2$. (a) Instantaneous velocity distribution superimposed on the dye visualization image from OFM; (b) instantaneous velocity distribution with velocity magnitude contour from OFM; (c) phaseaveraged velocity distribution over 200 trials for the same time step from OFM; (d) phase-averaged velocity distribution over 200 trials from PIV [(b)–(d) use the same velocity magnitude legend and reference vector; 8 × 8 vectors were skipped from OFM results].

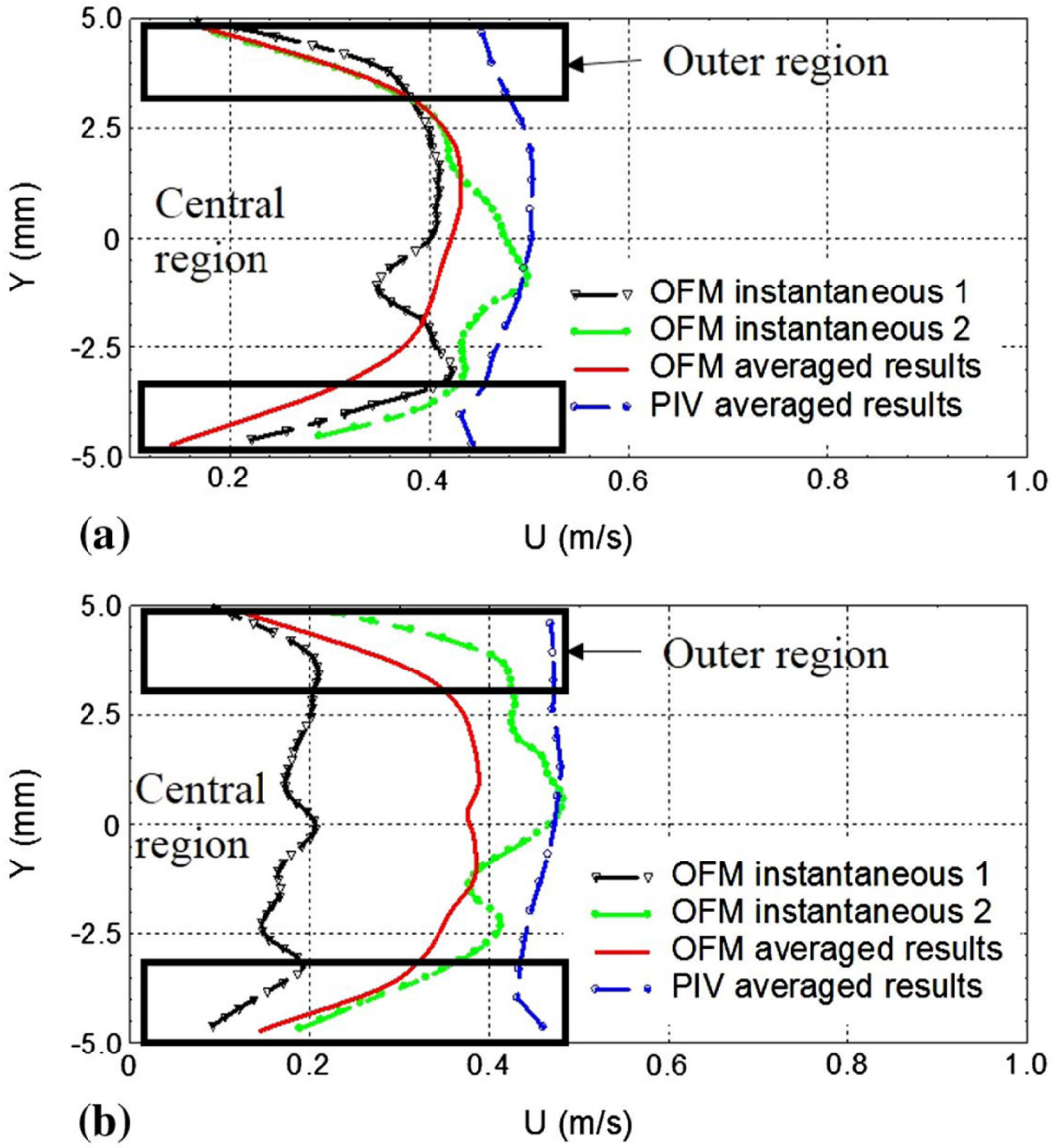

Fig. 6.

Velocity profiles comparison for OFM instantaneous velocity field, OFM averaged velocity field, and PIV averaged velocity field at (a) $X = 34$ mm and (b) $X = 42$ mm for $t/T = 0.2$.

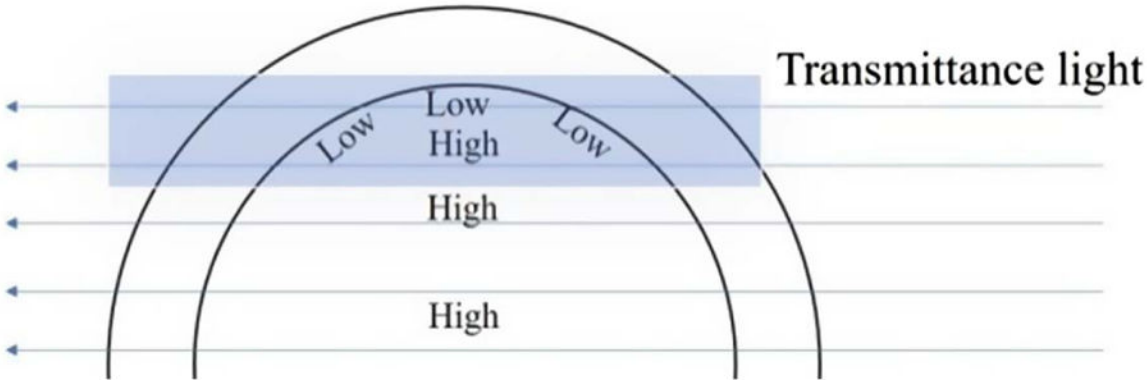

Fig. 7.

Demonstration of the transmittance light through the tube flow; low indicates low-speed region, and high indicates high-speed region.

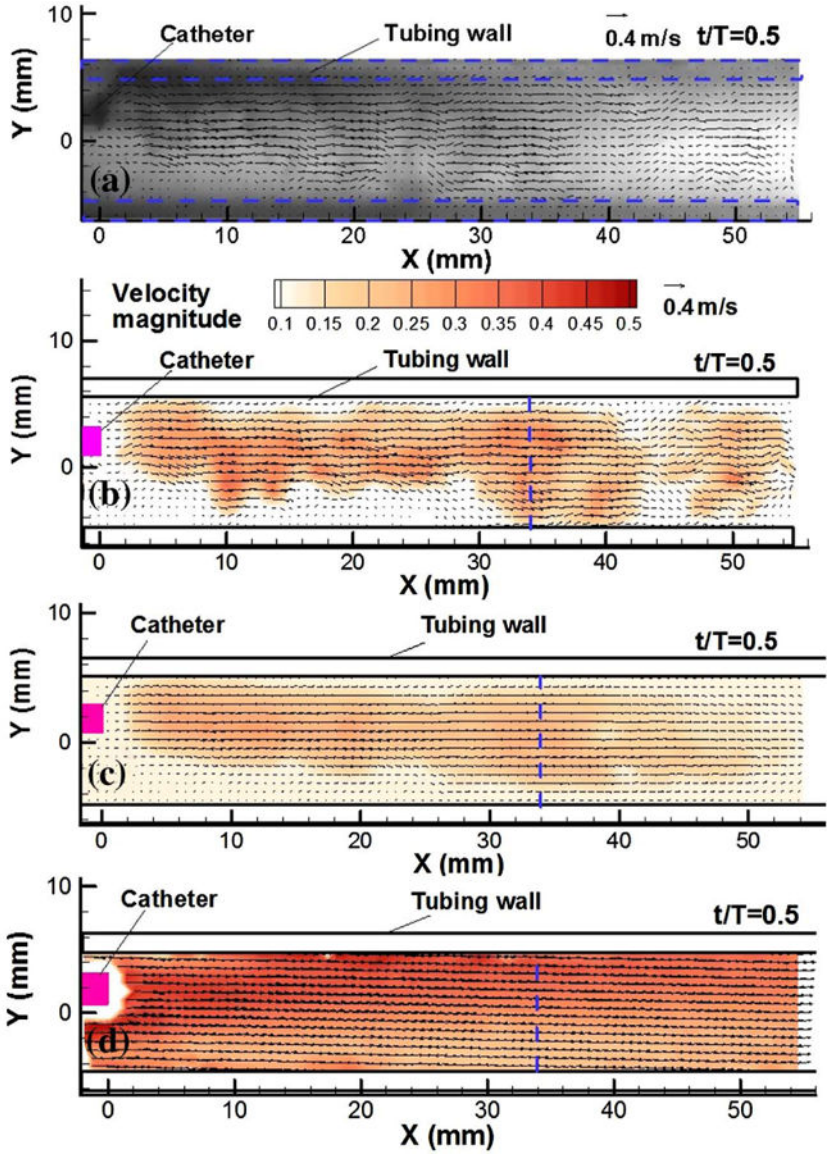

Fig. 8.

Velocity distribution results from OFM and PIV at $t/T = 0.5$. (a) Instantaneous velocity distribution superimposed on the dye visualization image from OFM; (b) instantaneous velocity distribution with velocity magnitude contour from OFM; (c) phase-averaged velocity distribution over 200 trials for the same time step from OFM; (d) phase-averaged velocity distribution over 200 trials from PIV [(b)–(d) use the same velocity magnitude legend and reference vector; 8 × 8 vectors were skipped from OFM results].

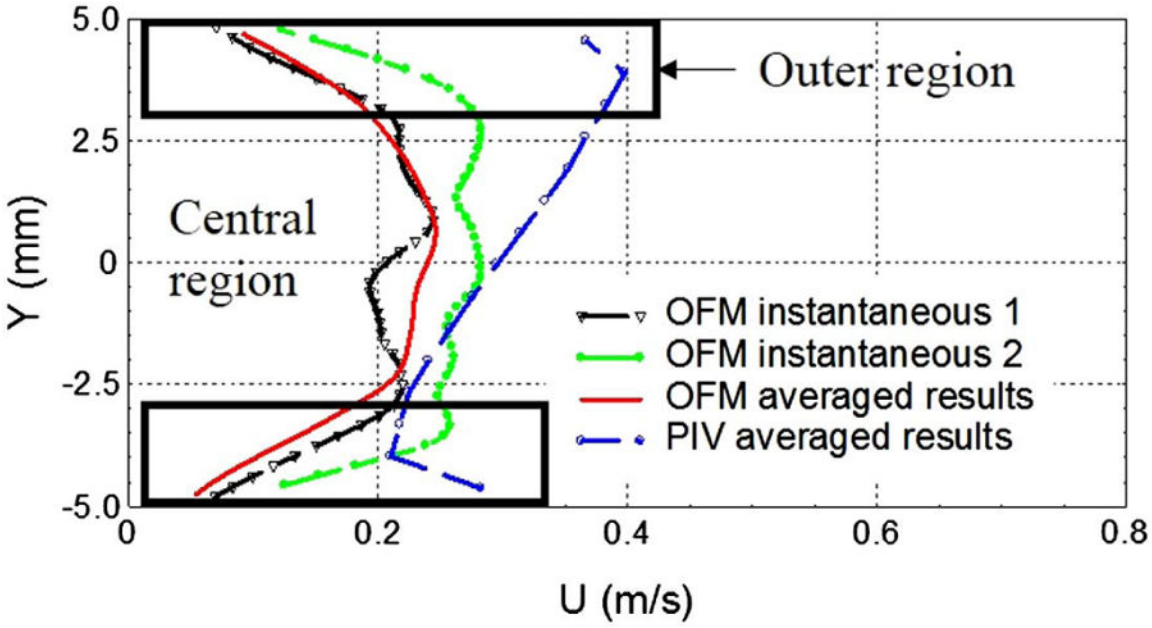

Fig. 9.

Velocity profiles comparison for OFM instantaneous velocity field, OFM averaged velocity field, and PIV averaged velocity field at $X = 34$ mm for $t/T = 0.5$.

Table 1.

Comparison of Averaged Velocity Magnitude in Central and Outer Regions, and Total Volume Flow Rate $\dot{Q}$ at X = 34 mm for t/T = 0.2 and 0.5

t/T	Dye Central(m/s)	PIV Central(m/s)	Error	Dye Outer(m/s)	PIV Outer(m/s)	Error	Dye $\dot{Q}$ (ml/s)	PIV $\dot{Q}$ (ml/s)	Error
0.2	0.41	0.49	16%	0.24	0.34	29%	24.4	29.9	18%
0.5	0.22	0.29	24%	0.13	0.23	43%	12.9	19.0	32%